Journal of Power Sources 196 (2011) 3583–3591

Contents lists available at ScienceDirect

Journal of Power Sources

journal homepage: www.elsevier.com/locate/jpowsour

High-temperature mechanical properties of a solid oxide fuel cell glass sealant in sintered forms

Hsiu-Tao Chang[a], Chih-Kuang Lin[a,*], Chien-Kuo Liu[b], Szu-Han Wu[b]

[a] Department of Mechanical Engineering, National Central University, Jhong-Li 32001, Taiwan
[b] Nuclear Fuel & Material Division, Institute of Nuclear Energy Research, Lung-Tan 32546, Taiwan

ARTICLE INFO

Article history:
Received 13 October 2010
Received in revised form
12 December 2010
Accepted 13 December 2010
Available online 21 December 2010

Keywords:
Planar solid oxide fuel cell
Sintered glass sealant
Ring-on-ring test
High temperature
Mechanical properties

ABSTRACT

High-temperature mechanical properties of a silicate-based glass sealant (GC-9) for planar solid oxide fuel cell have been studied in sintered forms. Ring-on-ring biaxial flexural tests are carried out at room temperature to 800 °C for the sintered GC-9 glass. The results are also compared with those in cast bulk forms. From the force–displacement curves, the glass transition temperature (T_g) of the non-aged, sintered GC-9 glass is estimated to be between 700 °C and 750 °C, while that of the aged one is between 750 °C and 800 °C. Due to a crack healing effect of the residual glass at high temperature, the flexural strength of the sintered GC-9 glass at temperature of 650 °C to T_g point is greater than that at room temperature. At temperature above T_g, the flexural strength and stiffness are considerably reduced to a level lower than the room-temperature one. The sintered GC-9 glass with pores and crystalline phases has a flexural strength lower than the cast bulk one at temperature of 650 °C and below. Due to a greater extent of crystallization, the flexural strength and stiffness of the sintered GC-9 glass are greater than those of the cast bulk one at 700–800 °C.

1. Introduction

Solid oxide fuel cells (SOFCs) provide an environment-friendly way of making electrical power with high efficiency from a variety of fuels [1–3]. As the typical operating temperature range for an SOFC is 600–1000 °C, selection of component materials becomes a very important issue. Among the SOFCs developed, the planar SOFC (pSOFC) has a lower manufacturing cost and higher power density. Reducing operating temperature is a recent tendency to lower material cost and enhance component durability and stability such that an intermediate operating temperature between 600 °C and 800 °C is a target for developing a practical pSOFC [3]. Sealants are important in a pSOFC to maintain a long-term operation and good performance. Sealants must separate the gases and maintain a gas-tight condition for a pSOFC during operation, and cannot react with other components. Match of coefficient of thermal expansion (CTE), compatibility, and long-term durability are important characteristics for selecting a suitable sealant for a pSOFC.

Glass and glass ceramic materials have stable performance during high-temperature operation so that they are among the favorable candidates to seal the components of a pSOFC [4,5]. Different glass and glass ceramic systems have been developed and evaluated for practical use in pSOFC [5,6]. Silicate glass systems with alkaline-earth modifiers are among the favorites because of their stable characteristics [5,6]. Besides, a self-healing feature of some glass systems has attracted more attention for pSOFC [7–11]. Such self-healing glasses have suitable viscosity such that they can not only heal cracks or defects at high temperatures but also relax stresses caused by thermal gradient or CTE mismatch. Generally, glass ceramic sealants can be made through crystallization of glasses by heat treating bulk glasses or sintering powdered glasses [12,13]. A typical crystallization heat-treatment includes nucleation and crystallization stages [12–14]. Different from crystallizing bulk glasses, the sintering approach starts from powders of a glass with sintering and crystallization taking place in the same thermal event. Such a sintering approach has a lower cost and easier utilization of the glass sealant than the bulk approach in which a significant proportion of cost results from machining for SOFC use. Therefore, practical application is carried out by the sintering approach and sealants are usually applied to pSOFC stacks with this method.

A glass sealant might fully or partially crystallize during the assembling or operating stage of pSOFCs to produce crystalline phases in the glass which is called glass ceramic. After the crystallization process, thermal, chemical and/or mechanical properties of a glass may be changed [15–19]. Such changes of material properties might influence its compatibility with other components, and the long-term stability and mechanical integrity of

* Corresponding author at: Department of Mechanical Engineering, National Central University, 300 Jhong-Da Rd., Jhong-Li 32001, Taiwan. Tel.: +886 3 426 7340; fax: +886 3 425 4501.
E-mail address: t330014@cc.ncu.edu.tw (C.-K. Lin).

0378-7753/$ – see front matter © 2010 Elsevier B.V. All rights reserved.
doi:10.1016/j.jpowsour.2010.12.035

a pSOFC stack. Only a few studies [6,8,9,20] have investigated the complex crystallization effect on the mechanical properties and related mechanisms for sintered, powdered glasses. Crystallization effect on the mechanical properties of a self-healing bulk $BaO–B_2O_3–Al_2O_3–SiO_2$ glass (designated as GC-9 glass) has been investigated for application in pSOFC [11]. Crystalline phases ($Ba_3La_6(SiO_4)_6$) are formed in the aged bulk GC-9 glass by a heat treatment at 900 °C for 3 h and the residual glass in the aged bulk GC-9 glass is also changed [11]. Through such a heat treatment, the glass transition temperature (T_g) of the aged bulk GC-9 glass sealant is reduced from 668 °C to 650 °C while the softening temperature (T_s) is increased from 745 °C to 826 °C [11]. Apparently, the residual glass in the aged bulk GC-9 glass is different from the original bulk GC-9 glass in terms of such variation in thermal properties. Even though crystallization changes the high-temperature mechanical properties, self-healing ability and stress relaxation phenomena are still present at high temperature for the aged bulk GC-9 glass [11]. However, crystallization mechanisms of powdered glasses by sintering, in which particle surfaces result in predominance of surface crystallization, differs from those in bulk glass ceramics [12,13]. As part of a series of studies [10,11] on the high-temperature mechanical properties of a glass sealant for pSOFC, the aim of this study is to investigate the high-temperature mechanical properties of the sintered, powdered GC-9 glass and make a comparison with those of the bulk GC-9 glass. Such high-temperature mechanical properties and behavior are important to design a reliable pSOFC stack. Systematic ring-on-ring tests were conducted at the temperature range of room temperature to 800 °C for powdered GC-9 glass after sintering (hereafter called sintered GC-9 glass) to investigate variation of the mechanical properties with temperature. Microstructural and fractography analyses were also conducted to correlate the mechanical properties with microstructural characteristics.

2. Experimental procedures

2.1. Glass forming and specimen preparation

The GC-9 glass sealant investigated in the study is a novel $BaO–B_2O_3–Al_2O_3–SiO_2$ glass which has been recently developed at the Institute of Nuclear Energy Research (INER) for use in pSOFC [21–25]. The thermal properties and chemical stability of this glass sealant for pSOFC applications have been investigated [21–23]. The high-temperature adherent and hermetic properties of the sintered GC-9 sealant have also been studied [24,25]. Overall, the GC-9 glass sealant shows good thermal properties, chemical compatibility with other components, stability, and hermetic properties to be well used in pSOFC [21–25].

Chemical composition of the GC-9 glass investigated includes 0–40 mol% BaO, 0–15 mol% B_2O_3, 0–10 mol% Al_2O_3, 0–40 mol% SiO_2, 0–15 mol% CaO, 0–15 mol% La_2O_3, and 0–5 mol% ZrO_2. The given GC-9 glass sealant was made by mixing the constituent oxide powders and melting at 1550 °C for 10 h. After melting, it was poured into a mold preheated to 680 °C to produce GC-9 glass ingots. The GC-9 glass ingots were then annealed at 680 °C for 8 h and cooled down to room temperature. GC-9 glass powders were made by crushing the as-cast glass ingots and sieved with 325 mesh sieves. The average powder size is 45 μm. Slurries were then made by adding into the GC-9 powders desired amounts of solvent (alcohol), binder (ethyl celluloid), and plasticizer (polyethylene glycol). After well mixing, the slurries were dried at 80 °C for 1 h and the dry mixture was ground into powders again. The GC-9 glass powders were then put into a mold and pressed to form a circular disk specimen with a diameter of 40 mm and thickness of 1.5 mm for ring-on-ring test. The circular disk-shape specimens were heat treated in air by the following steps: (1) heated from room temperature to 550 °C at 5 °C min^{-1}, (2) held at 550 °C for 1 h, (3) heated up to 850 °C at 5 °C min^{-1}, (4) sintered at 850 °C for 4 h, (5) cooled down to 750 °C at 5 °C min^{-1}, (6) held at 750 °C for 4 h, and (7) cooled down to room temperature. Specimens through such heat-treatment conditions are designated as non-aged, sintered GC-9 glass. Although they are called non-aged, sintered GC-9 glass, crystallization may take place in these specimens when sintered at 850 °C. Furthermore, in order to study the effect of crystallization with a longer aging time, some specimens were also prepared by the same heat-treatment profile, except the holding time at 750 °C. These specimens were held at 750 °C for 100 h instead of 4 h and they are designated as aged, sintered GC-9 glass. All of the specimens were polished with an 80-grit SiC paper to reduce surface roughness. After the sintering process, a boiling water technique [26] was used to determine the apparent porosity of the sintered GC-9 glass. The apparent porosity of the sintered GC-9 glass was around 5–7%. In addition, crystalline phases in the sintered GC-9 glass were determined by X-ray diffraction (XRD). Scanning electron microscopy (SEM) with an energy dispersive X-ray spectrometer (EDS) was applied to analyze the microstructure and crystalline morphology.

2.2. Measurement of mechanical properties

For determination of the strength of plate-like materials, biaxial flexural test is a suitable method because edge effects can be minimized. In the present study, a biaxial flexural ring-on-ring test following the test standard of ASTM C1499 [27] was applied to determine the mechanical properties of the non-aged and aged, sintered GC-9 specimens at different testing temperatures. The ring-on-ring tests were performed by using a commercial closed-loop servo-hydraulic machine attached with a furnace. The flexural loading fixture with a 10-mm-diameter inner loading ring and 20-mm-diameter outer supporting ring was made of alumina in order to perform tests at high temperatures. The testing temperatures were set at 25 °C, 650 °C, 700 °C, 750 °C, and 800 °C. For each high-temperature test, the specimen was heated to the specified temperature at a heating rate of 6 °C min^{-1}. The specimen was then held at the specified temperature for 3 min before applying the load. The load was applied under displacement control with a cross-head speed of 0.0005 mm s^{-1} for all the given testing temperatures. The load–displacement relationship was recorded for each test to calculate the flexural strength and other properties. Fracture surfaces of the broken specimens were observed with SEM to identify the fracture origins and mechanisms.

According to ASTM C1499 [27], the formula for the biaxial flexural strength, σ_f, of a circular plate is given as

$$\sigma_f = \frac{3P}{2\pi h^2}\left[(1-\nu)\frac{D_S^2 - D_L^2}{2D^2} + (1+\nu)\ln\frac{D_S}{D_L}\right] \quad (1)$$

where P is the maximum applied force, h is the thickness of specimen, and D_L, D_S, and D are the diameters of the load ring, support ring and specimen, respectively. In the present study, the Poisson's ratio $\nu = 0.3$ was used in Eq. (1). The deflection contour in the thickness direction from center to edge of the specimen was derived from a previous study [28] and is shown as

$$\delta = \frac{3P(1-\nu^2)R_L^2}{2\pi h^3 E}\left\{\left(\frac{R_S}{R_L}\right)^2 - 1 - \left[\left(\frac{R}{R_L}\right)^2 + 1\right]\ln\left(\frac{R_S}{R_L}\right) + \frac{1}{2}\frac{1-\nu}{1+\nu}\frac{R_S^2 - R_L^2}{R_{SP}^2}\frac{R_S^2 - R^2}{R_L^2}\right\} \quad \text{for} \quad 0 \le R \le R_L \quad (2)$$

where δ is the deflection of the specimen, R is the radial distance from the disk center to specified point, and R_L, R_S, R_{SP} are the radii of the load ring, support ring, and specimen. Rearrangement of

Eq. (2) and the Young's modulus of the sintered GC-9 glass can be calculated through the following formula

$$E = \frac{3P(1-\nu^2)R_L^2}{2\pi h^3 \delta}\left\{\left(\frac{R_S}{R_L}\right)^2 - 1 - \left[\left(\frac{R}{R_L}\right)^2 + 1\right]\ln\left(\frac{R_S}{R_L}\right) + \frac{1}{2}\frac{1-\nu}{1+\nu}\frac{R_S^2 - R_L^2}{R_{SP}^2}\frac{R_S^2 - R^2}{R_L^2}\right\} \quad (3)$$

The term $P\delta^{-1}$ can be determined from the slope of the force–displacement curve recorded in the ring-on-ring test.

2.3. Weibull statistic analysis

The Weibull statistics [29] is commonly used to describe the fracture behavior of brittle materials. Based on a weakest-link hypothesis, it is assumed that the most severe flaw controls the strength. When subjected to an applied stress, σ, the cumulative probability of failure for a brittle material can be expressed by [29]

$$F = 1 - \exp\left[-\left(\frac{\sigma - \sigma_u}{\sigma_0}\right)^m\right] \quad (4)$$

where F is the failure probability for an applied stress σ, σ_0 is the Weibull characteristic strength (which corresponds to $F = 63.2\%$, or a value of zero for $\ln\ln(1/(1-F))$), σ_u is the threshold stress (below which no failure will occur), and m is the Weibull modulus. Here, the Weibull modulus m is a measure of the degree of strength data dispersion. If σ_u is assumed to be zero, Eq. (4) becomes a two-parameter relation, as shown below [29]

$$F = 1 - \exp\left[-\left(\frac{\sigma}{\sigma_0}\right)^m\right] \quad (5)$$

This two-parameter Weibull probabilistic equation was applied to analyze the scattering of the strength data generated in the current study. In order to have enough data points for Weibull analysis, more than fifteen specimens were tested at each given testing condition.

3. Results and discussion

3.1. Microstructure of sintered glass ceramic

Crystalline phases of the aged bulk and sintered GC-9 glass were characterized by XRD. Fig. 1 shows the XRD patterns for the non-aged bulk GC-9 glass, aged bulk GC-9 glass, non-aged, sintered GC-9 glass, and aged, sintered GC-9 glass. As shown in Fig. 1, no phase peaks were found in the non-aged, as-cast bulk GC-9 glass indicating that it is a typically amorphous phase. However, there are several phase peaks present in the curves of the aged bulk GC-9 glass, non-aged, sintered GC-9 glass, and aged, sintered GC-9 glass indicating existence of certain crystalline phases in these materials. Apparently, a certain degree of crystallization was induced in the bulk GC-9 glass after an aging heat treatment [11]. The major phase peaks in the XRD pattern of the aged bulk GC-9 glass correspond to a structure of $Ba_3La_6(SiO_4)_6$ [11]. On the other hand, crystallization also took place in the sintered GC-9 glasses and the dominant crystalline phases are $BaSiO_3$ and alpha-$Ba(Al_2Si_2O_8)$ in addition to $Ba_3La_6(SiO_4)_6$. However, an aging time of 100 h did not generate additional crystalline phases in the sintered GC-9 glass.

SEM micrographs of the microstructure in the non-aged and aged, sintered GC-9 are shown in Fig. 2. Needle-shape crystals and aggregated particles were observed in both conditions. Needle-shape crystals are the primary crystalline phase, alpha-$Ba(Al_2Si_2O_8)$. In addition to XRD analysis, compositions of the needle-shape crystals were confirmed to include elements of Ba, Al, Si and O by EDS analysis in the SEM. As the aggregated particles are buried in the residual glass of the sintered GC-9 glass, it is difficult to identify their phases. Apparently, such a microstructural morphology is different from that in the aged bulk glass [11]. There was no microvoid inside the aged bulk GC-9 glass, but microvoids throughout the non-aged and aged, sintered GC-9 glass body were found as a result of burning of the binder and/or plasticizer during the sintering process. In addition, the size and amount of crystalline phases in the sintered GC-9 glass are greater than those in the aged bulk GC-9 glass. The bulk GC-9 glass crystallized only at nucleating agents in the material, but the major crystallization in the sintered GC-9 glass occurred at the surfaces of glass powders as well as at the nucleating agents. Therefore, the type, size, and amount of crystalline phase are different between the sintered and bulk GC-9 glass due to different nucleation sites of crystallization. The non-aged, sintered GC-9 glass exhibits pores (Fig. 2(a)), while pores in the aged, sintered GC-9 glass show a different morphology (Fig. 2(c)) after a longer aging treatment. In addition, re-crystalline phases are present on the original crystalline phases, as shown in Fig. 2(e). Although major crystalline phases were not changed in the sintered GC-9 glass after aging at 750 °C for 100 h, microvoids between needle-shape crystals and aggregated particles are filled with residual glass and/or re-crystalline phases.

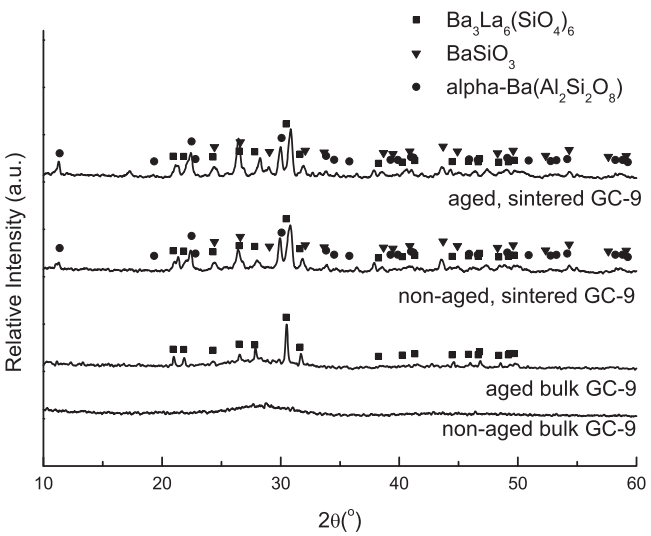

Fig. 1. XRD patterns of GC-9 glass in various forms.

3.2. Influence of environmental temperature on mechanical behavior

Fig. 3 shows the typical force–displacement curves for the non-aged and aged, sintered GC-9 glass at 25 °C, 650 °C, 700 °C, 750 °C, and 800 °C. Sintered GC-9 glass specimens were fractured at all given testing conditions. Even though some of them did not break to pieces at 750 °C or 800 °C, cracks were still generated on the tensile surfaces of these specimens. As cracks were formed, such specimens were also considered fractured. For the non-aged, sintered GC-9 glass at temperature 700 °C and below, the force–displacement curves remained almost linear until final fracture, while those for 750 °C and 800 °C were non-linear (Fig. 3(a)). However, the aged, sintered GC-9 glass exhibited more brittleness, as they showed a brittle fracture pattern at temperature up to 750 °C. At 800 °C, serrations in the force–displacement curve were found for the aged, sintered GC-9 glass.

Brittle fracture and stress relaxation both took place in the non-aged and aged, sintered GC-9 glass, but the transition tem-

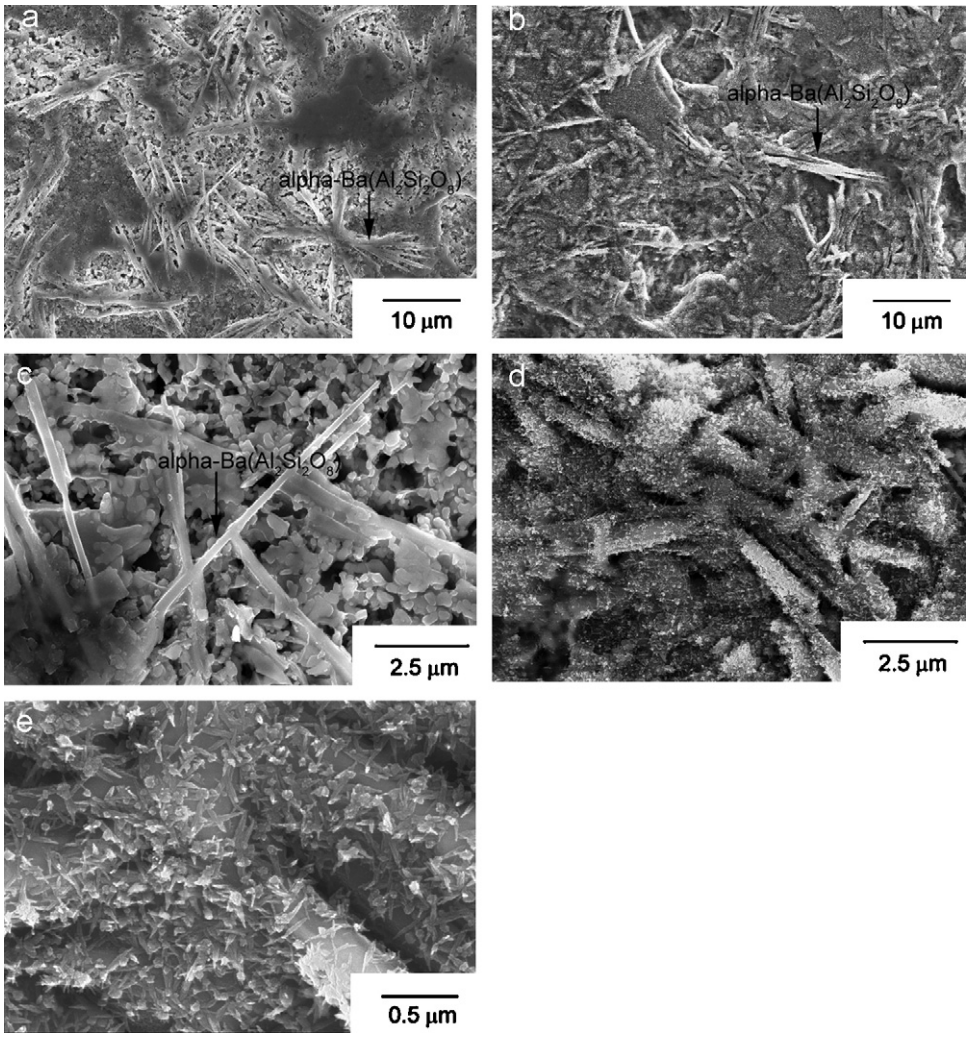

Fig. 2. Microstructure of sintered GC-9 glass: (a) non-aged condition; (b) non-aged condition in high magnification; (c) aged condition; (d) aged condition in high magnification; (e) aged condition in higher magnification.

perature from brittle to ductile fracture and the degree of stress relaxation were different. For the non-aged, sintered GC-9 glass, brittle fracture was observed at temperature 700 °C and below, and stress relaxation occurred at 750 °C and 800 °C. As described elsewhere [11], T_g of the aged bulk GC-9 glass is 650 °C which can be considered as a reference index of the transition temperature from brittle to ductile fracture for the sintered GC-9 glass. In the aged bulk GC-9 glass, the residual glass was the major phase to affect the high-temperature mechanical behavior when tested at or around T_g (650 °C). The non-aged, sintered GC-9 glass at 700 °C showed a brittle fracture pattern, but its stiffness was smaller than that at 25 °C and 650 °C. As the non-aged, sintered GC-9 glass has more crystalline phases than the aged bulk one so that its transition temperature is expected to be higher than 650 °C. As the force–displacement curve is linear at 700 °C and becomes non-linear at 750 °C for the non-aged, sintered GC-9 glass, its transition temperature is at least greater than 700 °C. For the aged, sintered GC-9 glass, its transition temperature is even higher than 750 °C, as its force–displacement curve becomes non-linear only at 800 °C. As the sintered GC-9 glass aged at 750 °C with a longer time (100 h) had a greater extent of crystallization, the transition temperature from brittle to ductile fracture was thus increased to be higher than 750 °C. It is clear that the degree of crystallization could affect the transition temperature of the given GC-9 glass.

Although stress relaxation occurred in the non-aged, sintered GC-9 glass at 750 °C and 800 °C (Fig. 3(a)), the stress–relaxation feature is different from that in the aged bulk GC-9 glass [11]. Note that the non-aged, sintered GC-9 glass has a microstructure consisting of crystalline phases and glassy matrix. For the non-aged, sintered GC-9 glass specimens tested at 750 °C and 800 °C, cracks were formed on the tensile surface at the first drop of force in the force–displacement curve. After this first force drop, these surface cracks continued to grow as the biaxial ring-on-ring test went on. At the same time, stress relaxation also took place during the test under a constant displacement rate of 0.0005 mm s^{-1}. Because of such a stress–relaxation mechanism, the cracked specimens did not break to pieces when the test was terminated. The stress–relaxation mechanism in the non-aged, sintered GC-9 glass may involve viscoelastic behavior of porous and glassy phases, crystallite/glass phase decohesion, microcracking and/or plasticity of the residual glassy phases [30].

For the aged, sintered GC-9 glass shown in Fig. 3(b), there was no stress relaxation at 750 °C, but there were serrations in the force–displacement curve at 800 °C. Such a serrated force–displacement curve implies that some surface cracks were formed at the first force drop, and growth of these cracks was presumably retarded by crystalline phases. Therefore, the applied force needed to be increased again to overcome these barriers for crack growth. Such a phenomenon repeated several times and the spec-

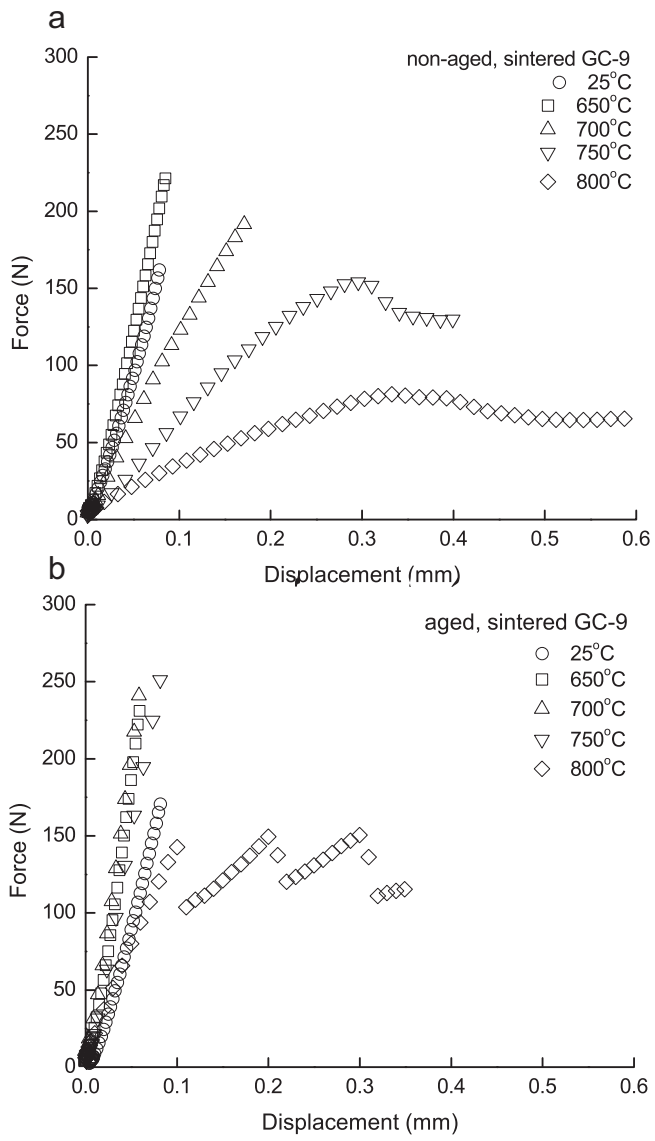

Fig. 3. Typical force–displacement relationships at various temperatures for (a) non-aged and (b) aged, sintered GC-9 glass.

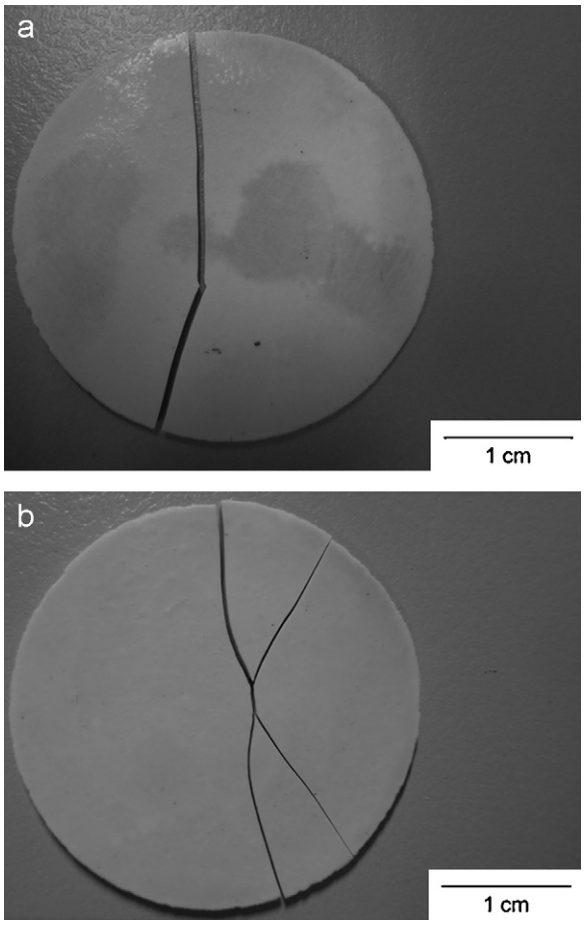

Fig. 4. Typical fracture patterns: (a) two pieces; (b) more than two pieces.

imen did not break to pieces when the test was terminated. In addition, stiffness in the linear region of the aged, sintered GC-9 glass at 750 °C and 800 °C is not significantly reduced from that at lower temperatures. As described above, degree of crystallization, re-crystallization, and pores filled with residual glass and re-crystalline phases all contribute to the influence on mechanical properties at high temperatures. With an increasing extent of crystallization, a less amount of residual glass is available to release the stress at high temperature. In this regard, there is no obvious stress–relaxation phenomenon in the aged, sintered GC-9 glass tested at 750 °C and 800 °C.

Number of broken pieces for the sintered GC-9 glass specimens varies with temperature. Specimens of the non-aged, sintered GC-9 glass at 25 °C were commonly broken to two pieces (Fig. 4(a)), while they were commonly broken to more than two pieces at 650 °C and 700 °C (Fig. 4(b)). From a fractographic point of view, the frequency of crack branching provides qualitative information about the amount of energy available for fracture. The more energy, the more branching will occur [29]. When the testing temperature was set at 750 °C and above, cracks were generated and propagated on the tensile surface of the non-aged, sintered GC-9 glass specimens, as shown in Fig. 5(a). Winding surface cracks can be seen at these temperatures, as shown in Fig. 5(a). In addition, a large flexural deflection was observed and specimens were not broken to pieces. The aged, sintered GC-9 glass showed a similar trend of failure pattern to that of the non-aged one at temperature of 700 °C and below. That is, the aged, sintered GC-9 glass specimens were typically broken to two pieces at 25 °C and broken to more than two pieces at 650 °C and 700 °C. However, some of them did not break to pieces at 750 °C, but cracks were still generated on the tensile surface with an extent of flexural deflection less than the corresponding non-aged one. When the testing temperature was increased to 800 °C, surface cracks were generated and grew on the tensile surface of the unbroken, aged, sintered GC-9 glass specimens (Fig. 5(b)). Note that a large flexural deflection was also observed for this case. Unlike the winding surface cracks in the non-aged, sintered GC-9 glass at 750 °C or 800 °C, the aged one exhibited somewhat straight surface cracks at 800 °C. The difference in the failure pattern between the non-aged and aged, sintered GC-9 glass at 750 °C and 800 °C is attributed to different extents of crystallization.

3.3. Fracture strength and Weibull statistics

The two-parameter Weibull distribution of flexural strength for the sintered GC-9 glass at different temperatures is shown in Fig. 6. Table 1 lists the characteristic strength (σ_0) and Weibull modulus (m) for the bulk and sintered GC-9 glass at various temperatures. In Table 1, data of the bulk GC-9 glass are taken from a previous study [11] for comparison. As shown in Fig. 6(a) and Table 1, the non-aged, sintered C-9 glass exhibited a greater strength at 650 °C and 700 °C than that at room temperature due to a crack healing

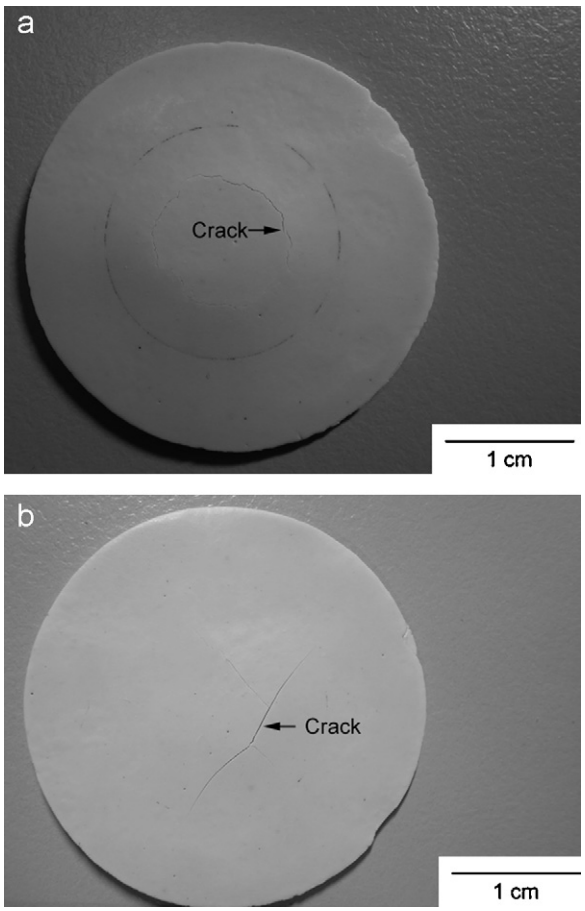

Fig. 5. Typical cracking patterns: (a) non-aged, sintered GC-9 glass tested at 750 °C and 800 °C; (b) aged, sintered GC-9 glass tested at 800 °C.

effect similar to that in the bulk GC-9 glass [10,11]. As compared to the aged bulk GC-9 glass, the non-aged, sintered GC-9 glass has a lower flexural strength at temperature of 650 °C and below, but has a higher flexural strength at 700 °C and above. It is due to a higher degree of crystallization in the non-aged, sintered GC-9 glass. Generally, crystalline phases in the glass and glass ceramic can enhance mechanical strength, but glasses and glass ceramics are sensitive to defects at low temperature. As the non-aged, sintered GC-9 glass has more pores generated during sintering process, its strength is lower than that of the aged bulk GC-9 glass at temperature of 650 °C and below. The flexural strength of the non-aged, sintered GC-9 glass at 700 °C is almost the same as that at 650 °C. When the testing temperature was increased to 700 °C, the viscous residual glass in the aged bulk GC-9 glass was the major factor to lower the flexural strength. However, crystalline phases in the non-aged, sintered GC-9 glass dominated the flexural strength at high temperature such that the flexural strength of this material at 650 °C and 700 °C was greater than that at room temperature.

Fig. 7 shows the typical fracture origins in the sintered GC-9 glass specimens. Arrows in the given micrographs indicate the fracture origins. There are many pores with different sizes in the volume of the non-aged and aged, sintered GC-9 glass. Because of these inherent defects, the sintered GC-9 glass exhibited a different fracture feature from the bulk GC-9 glass one [11]. Both the non-aged and aged, sintered GC-9 glass specimens were sensitive to these types of defects on the tensile surface, while the bulk GC-9 glass specimens were sensitive to the surface defects induced by machining. Such sintering pores on the tensile surface are stress concentrating sites favorable for fracture to initiate. The shape of these defects is irregular and their size varies from specimen to specimen. When the testing temperature was at or above 750 °C, stress relaxation started to influence and reduce the high-temperature strength of the non-aged, sintered GC-9 glass. As a result, the flexural strength of the non-aged, sintered GC-9 glass at 750 °C and 800 °C is decreased to a level less than that at room temperature.

For the aged, sintered GC-9 glass shown in Fig. 6(b) and Table 1, it has a greater flexural strength at 650 °C, 700 °C, and 750 °C than that at room temperature due to the aforementioned crack healing effect [10,11]. The flexural strength at these three temperatures can be seen as comparable, as the data points are almost merged together in Fig. 6(b). Note that the flexural strength of the aged, sintered GC-9 glass at 750 °C is significantly greater than that of the non-aged, sintered one. This, again, can be attributed to a greater extent of crystallization due to a longer aging time. Despite a higher degree of crystallization, the aged, sintered GC-9 glass still has many sintering defects and is also sensitive to these defects. It shows a more brittle behavior at 750 °C and 800 °C in comparison with the non-aged one since there is a less amount of viscous residual glass to release stresses. Although the flexural strength of the non-aged, sintered GC-9 glass at 800 °C is significantly reduced, it was still superior to the aged bulk GC-9 glass due to the existence of stronger crystalline phases. Both the non-aged and aged, sintered GC-9 glass crystallized and became glass ceramic after the given sintering process and heat treatments. It is obvious that the crystalline phases in the sintered GC-9 glasses strengthen the high-temperature mechanical properties in comparison with the bulk GC-9 glass. In spite of that, the residual glass phase still played a certain role in relaxing stresses at high temperature for both the non-aged and aged, sintered GC-9 glass.

Unlike the case of the bulk GC-9 glass, the Weibull moduli of the non-aged and aged, sintered GC-9 glass at 650 °C and above

Table 1
Weibull characteristic strength (σ_0) and Weibull modulus (m) for GC-9 glass at various temperatures.

Material	Temperature						
	25 °C	550 °C	600 °C	650 °C	700 °C	750 °C	800 °C
σ_0 (MPa)							
Non-aged bulk GC-9 glass	68	76	83	88	45[a]	4[a]	–
Aged bulk GC-9 glass	78	102	101	123	10[a]	2[a]	–
Non-aged, sintered GC-9 glass	42	–	–	54	51	36	19
Aged, sintered GC-9 glass	41	–	–	53	63	59	34
m							
Non-aged bulk GC-9 glass	7.7	9.7	7.5	10	–	–	–
Aged bulk GC-9 glass	4.5	10.7	11.3	7.2	–	–	–
Non-aged, sintered GC-9 glass	4.0	–	–	5.2	5.0	6.0	5.8
Aged, sintered GC-9 glass	5.5	–	–	5.0	4.8	4.9	6.0

Note: Data of the bulk GC-9 glass are from Ref. [11].
[a] Maximum flexural stress applied during test.

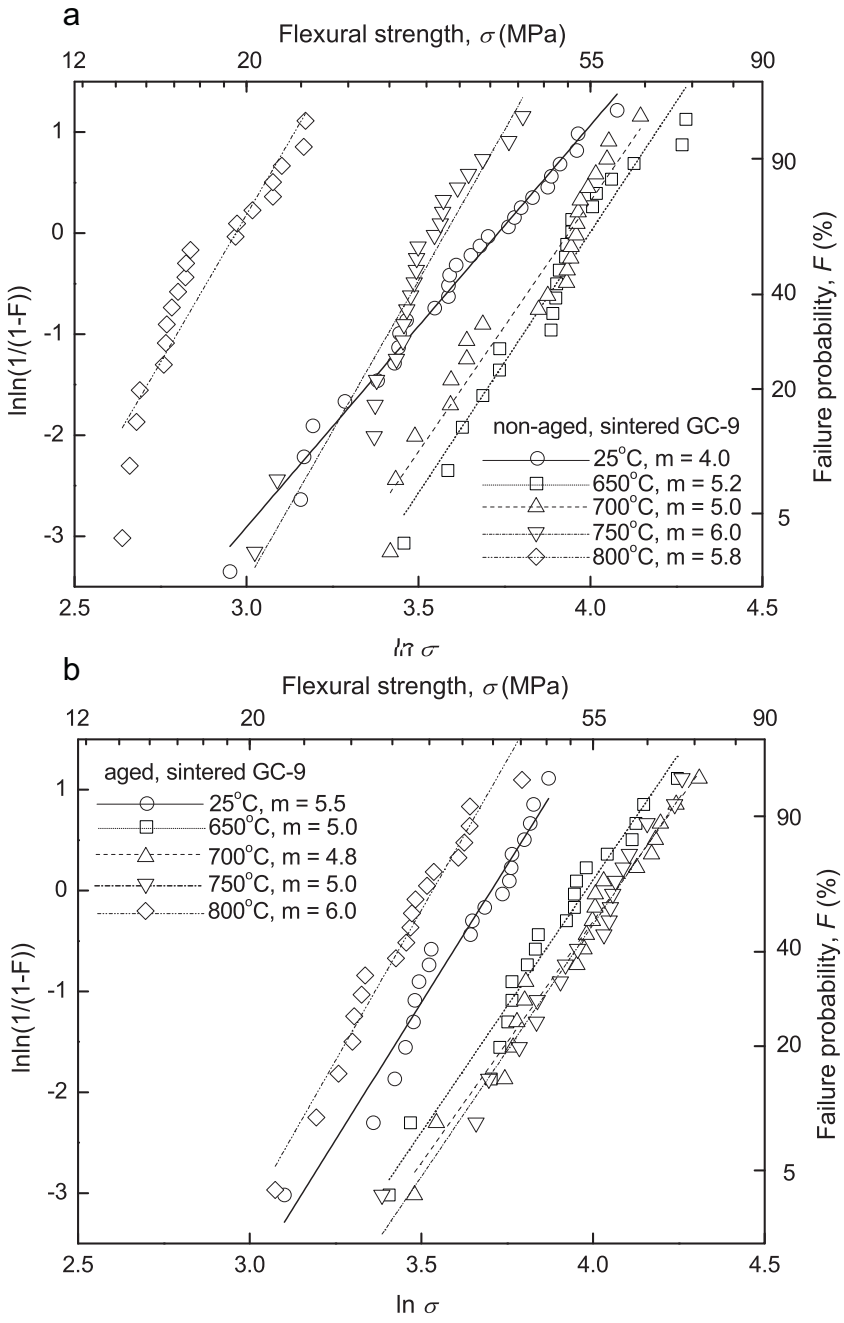

Fig. 6. Weibull distribution of flexural strength: (a) non-aged, sintered GC-9; (b) aged, sintered GC-9 (the unit of σ is MPa).

are barely greater than that at room temperature. As shown in Fig. 6(b) and Table 1, the values of the Weibull modulus for the sintered GC-9 glass in both non-aged and aged conditions can be seen as comparable. It implies that the outlines of the defects in the sintered GC-9 glass specimens at high temperatures were not significantly improved by the aforementioned crack healing effect to a similar extent in the bulk GC-9 ones. This may be attributed to a less amount of viscous residual glass in the sintered GC-9 glass, as compared to the aged bulk GC-9 glass. As the sintered GC-9 glass has more defects such that its Weibull modulus is smaller and flexural strength data are more dispersive in comparison to the bulk GC-9 glass. Even though the amount of residual glass in the non-aged and aged, sintered GC-9 glass is less than that in the bulk GC-9 glass, it could still relax the stress concentrations around flaws leading to a greater fracture strength at high temperature over room temperature.

3.4. Influence of environmental temperature on Young's modulus

The calculated Young's moduli (average value and standard deviation) for the bulk and sintered GC-9 glass at various temperatures are shown in Table 2. Note that data of the bulk GC-9 glass are taken from a previous study [11] for comparison. As there was significant stress relaxation at 750 °C for both the non-aged and aged bulk GC-9 glass, their Young's modulus could not be determined at this temperature and above [11]. For a given temperature, the Young's modulus of the non-aged, sintered GC-9 glass is lower than that of the non-aged bulk GC-9 glass, as shown in Table 2. The Young's moduli of the sintered GC-9 glass were determined from the force–displacement curves by testing the sintered specimens containing pores and defects. Sintered glass ceramics generally have more defects and pores than cast glasses such that their stiffness is influenced by the porosity in the material. Young's modulus

Table 2
Average value and standard deviation of Young's modulus for GC-9 glass at various temperatures.

Material	Temperature						
	25 °C	550 °C	600 °C	650 °C	700 °C	750 °C	800 °C
Young's modulus (GPa)							
Non-aged bulk GC-9 glass	66 (7.9)	66 (8.3)	64 (6.8)	59 (5.4)	17 (7.0)	–	–
Aged bulk GC-9 glass	68 (6.3)	71 (9.6)	72 (4.3)	47 (12)	2.6 (1.6)	–	–
Non-aged, sintered GC-9 glass	18 (5.8)	–	–	19 (3.3)	9.4 (2.2)	4.9 (1.9)	2.1 (0.7)
Aged, sintered GC-9 glass	19 (4.2)	–	–	24 (4.0)	22 (4.2)	17 (2.4)	6.5 (1.1)

Note: Data of the bulk GC-9 glass are from Ref. [11].
Note: Values in parentheses are the standard deviations.

of glass ceramics usually decreases with increasing porosity [31]. This might explain why the Young's modulus of the non-aged, sintered GC-9 glass is lower than that of the non-aged bulk GC-9 glass.

The Young's modulus of the non-aged, sintered GC-9 glass did not change when the temperature was increased from room temperature to 650 °C. However, it was significantly reduced at temperature of 700 °C and above. It is obvious that such a non-aged, sintered glass lost its stiffness at 700 °C and above due to the existence of residual glass. Again, T_g of the aged bulk GC-9 glass is 650 °C. Viscosity of such a glass significantly changed at temperature of 650 °C and above and the stiffness was also reduced. On the other hand, the aged, sintered GC-9 glass exhibited a slight increase of Young's modulus with temperature from room temperature to 650 °C. Above 650 °C, the Young's modulus of the aged, sintered GC-9 glass was decreased with increasing temperature. In particular, a significant drop took place at 750 °C which is higher than that of 700 °C in the non-aged, sintered one. For a given temperature, the aged, sintered GC-9 glass always has a greater Young's modulus than does the non-aged, sintered one due to a greater extent of crystallization. At the expected operation temperature range for a pSOFC, 700–800 °C, the sintered, powdered form of GC-9 glass has greater stiffness than does the cast bulk form. Apparently, a greater amount of crystalline phases could enhance the mechanical strength and stiffness for the given GC-9 glass at the operating temperature range of 700–800 °C.

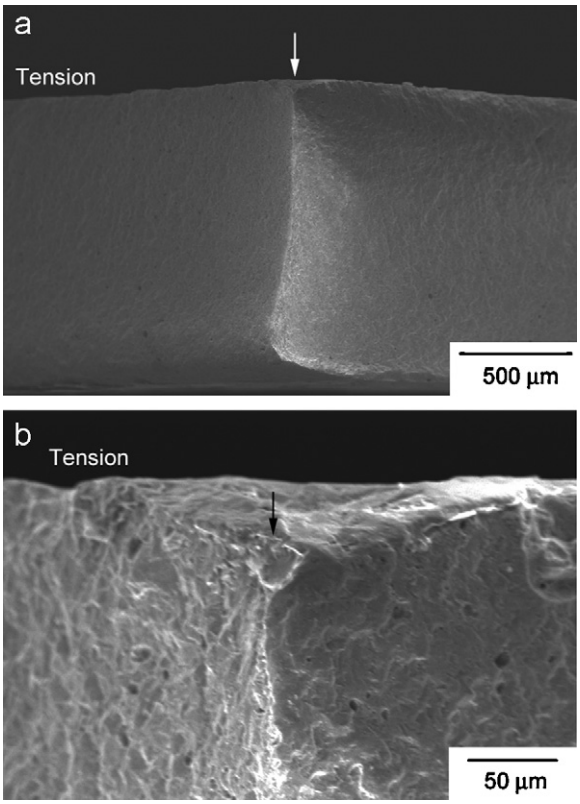

Fig. 7. Typical fracture origin in the sintered GC-9 glass specimens: (a) overview; (b) high magnification (arrows indicate the fracture origin).

4. Conclusions

In comparison with the cast, bulk form, more crystalline phases are formed in the sintered, powdered GC-9 glass because of a difference in crystallization process. The extent of crystallization is increased with aging time, but the types of crystalline phases are not changed in the sintered GC-9 glass. Based on the force–displacement curves of the sintered GC-9 glass, the glass transition temperature of the non-aged condition is estimated to be within the range of 700–750 °C, while it is within the range of 750–800 °C for the aged one.

For the sintered GC-9 glass, there is a flexural strength improvement with increasing temperature at temperature below the glass transition temperature because of a crack healing effect from the residual glass in the material. At temperature above the glass transition temperature, both flexural strength and Young's modulus are significantly decreased with increasing temperature. However, a greater flexural strength and stiffness of the aged, sintered GC-9 glass over the non-aged one is observed at temperature higher than 700 °C due to a greater extent of crystallization.

Due to the existence of a greater number of pores in the volume, the sintered GC-9 glass has a lower flexural strength and Young's modulus than does the cast bulk one at temperature below 700 °C. However, at temperature of 700–800 °C (expected operation temperature of pSOFC), the sintered GC-9 glass has a greater flexural strength and stiffness over the cast bulk one.

Acknowledgements

This work was supported by the National Science Council (Taiwan) under Contract No. NSC 95-2221-E-008-004-MY3 and by the Institute of Nuclear Energy Research (Taiwan) under Contract No. 992001INER047.

References

[1] M.A.J. Cropper, S. Geiger, D.M. Jollie, J. Power Sources 131 (2004) 57–61.
[2] N.Q. Minh, Solid State Ionics 171 (2004) 271–277.
[3] A. Weber, E. Ivers-Tiffée, J. Power Sources 127 (2004) 273–283.
[4] P.A. Lessing, J. Mater. Sci. 42 (2007) 3465–3476.
[5] J.W. Fergus, J. Power Sources 147 (2005) 46–57.
[6] K.D. Meinhardt, D.-S. Kim, Y.-S. Chou, K.S. Weil, J. Power Sources 182 (2008) 188–196.
[7] R.N. Singh, Int. J. Appl. Ceram. Technol. 4 (2007) 134–144.
[8] N. Govindaraju, W.N. Liu, X. Sun, P. Singh, R.N. Singh, J. Power Sources 190 (2009) 476–484.
[9] E.V. Stephens, J.S. Vetrano, B.J. Koeppel, Y. Chou, X. Sun, M.A. Khaleel, J. Power Sources 193 (2009) 625–631.
[10] H.-T. Chang, C.-K. Lin, C.-K. Liu, J. Power Sources 189 (2009) 1093–1099.
[11] H.-T. Chang, C.-K. Lin, C.-K. Liu, J. Power Sources 195 (2010) 3159–3165.
[12] J. Hlavac, Technology of Glass and Ceramics, Elsevier Science Publishing Company, Inc., New York, USA, 1983.

[13] M.H. Lewis, Glasses and Glass-Ceramics, Chapman and Hall Ltd., New York, USA, 1989.
[14] I.W. Donald, J. Mater. Sci. 28 (1993) 2841–2886.
[15] Z. Strnad, Glass-Ceramic Materials, Elsevier Science Publishing Company, Inc., New York, USA, 1986.
[16] D.G. Burnett, R.W. Douglas, Discuss. Faraday Soc. 50 (1970) 200–205.
[17] D.G. Burnett, R.W. Douglas, Phys. Chem. Glasses 12 (1971) 117–124.
[18] J.E. Shelby, Introduction to Glass Science and Technology, 2nd ed., Royal Society of Chemistry, New York, USA, 2005.
[19] R. Hill, P. Gilbert, J. Am. Ceram. Soc. 76 (1993) 417–425.
[20] W. Liu, X. Sun, M.A. Khaleel, J. Power Sources 185 (2008) 1193–1200.
[21] C.-K. Liu, T.-Y. Yung, K.-F. Lin, Proceedings of the Annual Conference of the Chinese Ceramic Society 2007 (CD-ROM), 2007 (in Chinese).
[22] C.-K. Liu, T.-Y. Yung, S.-H. Wu, K.-F. Lin, Proceedings of the MRS_Taiwan Annual Meeting 2007 (CD-ROM), 2007 (in Chinese).
[23] C.-K. Liu, T.-Y. Yung, K.-F. Lin, Proceedings of the Annual Conference of the Chinese Ceramic Society 2008 (CD-ROM), 2008 (in Chinese).
[24] C.-K. Liu, K.-C. Tsai, K.F. Lin, S.-H. Wu, T.-Y. Yung, Proceedings of the Annual Conference of the Chinese Ceramic Society 2009 (CD-ROM), 2009 (in Chinese).
[25] C.-K. Liu, T.-Y. Yung, K.-F. Lin, R.-Y. Lee, S.-H. Wu, ECS Trans. 25 (2009) 1491–1500.
[26] ASTM Standard C20, Standard Test Methods for Apparent Porosity, Water Absorption, Apparent Specific Gravity, and Bulk Density of Burned Refractory Brick and Shapes Boiling Water, ASTM International, West Conshohocken, PA, USA, 2008.
[27] ASTM Standard C1499-08, Standard Test Method for Monotonic Equibiaxial Flexural Strength of Advanced Ceramics at Ambient Temperature, ASTM International, West Conshohocken, PA, USA, 2008.
[28] R.W. Schmitt, K. Blank, G. Schönbrunn, Sprechsaal 116 (1983) 397–409 (in German).
[29] D.W. Richerson, Modern Ceramic Engineering, 2nd ed., Marcel Dekker, Inc., New York, USA, 1992.
[30] B.N. Nguyen, B.J. Koeppel, S. Ahzi, M.A. Khaleel, P. Singh, J. Am. Ceram. Soc. 89 (2006) 1358–1368.
[31] R.W. Davidge, Mechanical Behavior of Ceramics, Cambridge University Press, New York, USA, 1979.